THE JOURNAL OF CHEMICAL PHYSICS **143**, 234107 (2015)

Spin-flip, tensor equation-of-motion configuration interaction with a density-functional correction: A spin-complete method for exploring excited-state potential energy surfaces

Xing Zhang and John M. Herbert[a)]
Department of Chemistry and Biochemistry, The Ohio State University, Columbus, Ohio 43210, USA

(Received 9 September 2015; accepted 30 November 2015; published online 17 December 2015)

We revisit the formalism of the spin-adapted, spin-flip (SA-SF) configuration-interaction singles (CIS) method based on a tensor equation-of-motion formalism that affords proper spin eigenstates without sacrificing single-reference simplicity. Matrix elements for SA-SF-CIS are then modified in a manner similar to collinear spin-flip time-dependent density functional theory (SF-TDDFT), to include a DFT exchange-correlation correction. The performance of this method, which we call SA-SF-DFT, is evaluated numerically and we find that it systematically improves the energies of electronic states that exhibit significant spin contamination within the conventional SF-TDDFT approach. The new method cures the state assignment problem that plagues geometry optimizations and *ab initio* molecular dynamics simulations using traditional SF-TDDFT, without sacrificing computational efficiency, and furthermore provides correct topology at conical intersections, including those that involve the ground state, unlike conventional TDDFT. As such, SA-SF-DFT appears to be a promising method for generating excited-state potential energy surfaces at DFT cost. © *2015 AIP Publishing LLC*. [http://dx.doi.org/10.1063/1.4937571]

I. INTRODUCTION

Spin-flip time-dependent density functional theory[1,2] (SF-TDDFT) is a qualitatively correct and very efficient electronic structure method for describing electronic excitation energies,[1–7] conical intersections,[8,9] excited-state reaction pathways,[9–19] and excited-state non-adiabatic *ab initio* molecular dynamics (MD) simulations.[20,21] Spin-flipping excitations enable SF-TDDFT to treat ground- and excited-state electron correlation on the same footing, while also incorporating some doubly-excited determinants that are important for biradicals.[1,22] The dynamical correlation that is included in SF-TDDFT makes this model more accurate than its wavefunction analogue, spin-flip configuration-interaction singles (SF-CIS).[22]

Despite these favorable features, SF-TDDFT has one notorious drawback in the form of serious spin contamination. This can easily be understood using an example in which a high-spin triplet reference state is used in order to target singlet states obtained from a single $\alpha \rightarrow \beta$ spin-flip excitation. Figure 1 depicts all possible electron configurations obtained in such a scenario, using a model consisting of four electrons in four orbitals. Only those excitations within the open-shell space are able to generate spin-pure solutions, whereas all other configurations are missing their "spin complements," leading to spin-contaminated solutions. In this example, at most three singlet states and one triplet state may exhibit proper spin symmetry, whereas all other solutions will be significantly spin-contaminated. This is a serious drawback in SF-TDDFT, especially for *ab initio* MD or excited-state optimizations, where states may cross as the molecular geometry is changed and some form of state-tracking is required. Since the number of spin-pure states is limited, only a few low-lying states can be studied in SF-TDDFT simulations,[20,21] and various techniques are required in order to follow the state having the desired spin symmetry.[20]

Several approaches have been proposed to generate spin eigenstates for open-shell TDDFT. Vahtras and Rinkevicius[23] introduced general excitation operators that can be used to generate excited states having well-defined spin multiplicities, whereas Li and Liu[24–26] extended the tensor equation-of-motion (TEOM) formalism, originally developed by Rowe and Ngo-Trong in nuclear physics,[27] to the case of molecular systems. At the SF-CIS level, Sherrill and co-workers[28] presented a spin-complete implementation within a restricted active space formalism, and Tsuchimochi *et al.*[29,30] reported a spin-projected formulation of SF-CIS in which spin-adapted solutions are also obtained. None of these approaches, however, has been applied to SF-TDDFT, which is the topic of the present work. We will derive a spin-adapted, spin-flip CIS (SA-SF-CIS) method based on one of three formally equivalent TEOMs.[27] To incorporate dynamical electron correlation, we will then go on to include a DFT correction, following along the lines that Grimme *et al.*[31,32] used to merge DFT with multireference configuration interaction (MRCI) in the DFT/MRCI method. The performance of this new method is then analyzed through some example calculations.

II. THEORY

We briefly review the TEOM formalism introduced by Rowe and Ngo-Trong,[27] then derive the working equations for SA-SF-CIS based on this formalism.

[a)] herbert@chemistry.ohio-state.edu

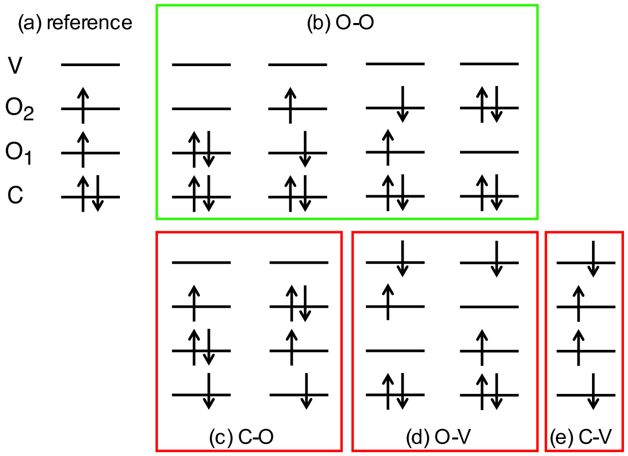

FIG. 1. Example of spin-flip from a high-spin triplet reference state, for a model system consisting of four electrons in four orbitals. Configuration (a) is the reference state. Configurations in (b) are obtained by a single flip-down excitation within the open-shell orbitals; only these configurations are able to form spin eigenstates. Configurations in (c)–(e) are obtained by closed- to open-shell excitations, open-shell to virtual excitations, and closed-shell to virtual excitations, respectively, each with a $\alpha \to \beta$ spin-flip excitation. These configurations are missing their complementary spin configurations and lead to spin-contaminated solutions in conventional SF-TDDFT.

A. Notation

The following notation is used throughout this work. Doubly- and singly-occupied molecular orbitals are labeled as $\phi_i, \phi_j, \phi_k, \phi_l, \ldots$ and $\phi_t, \phi_u, \phi_v, \phi_w, \ldots$, respectively, while virtual molecular orbitals are labeled as $\phi_a, \phi_b, \phi_c, \phi_d, \ldots$. We label arbitrary (occupied or virtual) molecular orbitals as $\phi_p, \phi_q, \phi_r, \phi_s, \ldots$. All two-electron integrals will be written in physicists' notation. Furthermore, we will use C, O, and V to denote closed, open, and virtual spaces, respectively, consistent with Fig. 1. A tensor operator having rank Γ is denoted as $\hat{O}^\dagger(\Gamma)$ and its μth component is $\hat{O}^\dagger(\Gamma, \mu)$.

B. Tensor equations of motion

The traditional scalar equations of motion[33] can be generalized to tensor equations of motion in a straightforward way using tensor basis functions instead of scalar basis functions.[27] One seeks the tensor operators $\hat{O}^\dagger_{x\lambda}$ with rank λ that relate the excited tensor state $|xS_f\rangle\rangle$ to some reference tensor state $|S_0\rangle\rangle$ in the following way:

$$\{\hat{O}^\dagger_{x\lambda} \times |S_0\rangle\rangle\}^{S_f} = |xS_f\rangle\rangle, \tag{1}$$

$$\hat{O}_{x\lambda}|S_0\rangle\rangle = 0. \tag{2}$$

We use curly brackets to represent the coupled products between two tensors, and the superscript above the bracket is the rank of the product tensor. The labels S_0 and S_f indicate the spin symmetries of the initial (reference) state and the final (target) state, respectively. (Note that S_0 as used in Section II does not mean "singlet ground state," S$_0$. The latter notation is used in the numerical calculations in Section III.) In Eq. (2), all possible coupled products should vanish. The tensor operator $\hat{O}^\dagger_{x\lambda}$ can be expanded by a series of tensor operators with different ranks,

$$\hat{O}^\dagger_{x\lambda} = \sum_i \hat{O}^\dagger_{x\lambda_i}, \tag{3}$$

and the ranks λ_i must satisfy the triangle relations required by Eq. (1), namely,

$$|S_0 - S_f| \le \lambda_i \le |S_0 + S_f|. \tag{4}$$

As shown by Rowe and Ngo-Trong,[27] three formally equivalent TEOMs can be derived from Eqs. (1) and (2). The first of these is

$$\begin{aligned}&\sum_{ij\Gamma}(-1)^{S_0-S_f-\Gamma-\lambda_i}(2\Gamma+1)^{1/2}W(\lambda_i\lambda_j S_0 S_0;\Gamma S_f)\langle S_0\|\{\hat{\bar{O}}_{y\lambda_i}\times[\hat{H},\hat{O}^\dagger_{x\lambda_j}]\}^\Gamma\|S_0\rangle\\&\quad=\omega_{xS_f}\sum_{ij\Gamma}(-1)^{S_0-S_f-\Gamma-\lambda_i}(2\Gamma+1)^{1/2}W(\lambda_i\lambda_j S_0 S_0;\Gamma S_f)\langle S_0\|\{\hat{\bar{O}}_{y\lambda_i}\times\hat{O}^\dagger_{x\lambda_j}\}^\Gamma\|S_0\rangle.\end{aligned} \tag{5}$$

The second version is

$$\begin{aligned}&\sum_{ij\Gamma}(-1)^{S_0-S_f-\Gamma-\lambda_i}(2\Gamma+1)^{1/2}W(\lambda_i\lambda_j S_0 S_0;\Gamma S_f)\langle S_0\|\{[\hat{\bar{O}}_{y\lambda_i},[\hat{H},\hat{O}^\dagger_{x\lambda_j}]]\}^\Gamma\|S_0\rangle\\&\quad=\omega_{xS_f}\sum_{ij\Gamma}(-1)^{S_0-S_f-\Gamma-\lambda_i}(2\Gamma+1)^{1/2}W(\lambda_i\lambda_j S_0 S_0;\Gamma S_f)\langle S_0\|\{[\hat{\bar{O}}_{y\lambda_i},\hat{O}^\dagger_{x\lambda_j}]\}^\Gamma\|S_0\rangle.\end{aligned} \tag{6}$$

Finally, the third TEOM is

$$\begin{aligned}&\sum_{ij\Gamma}(-1)^{S_0-S_f-\Gamma-\lambda_i}(2\Gamma+1)^{1/2}W(\lambda_i\lambda_j S_0 S_0;\Gamma S_f)\langle S_0\|\{[\hat{\bar{O}}_{y\lambda_i},\hat{H},\hat{O}^\dagger_{x\lambda_j}]\}^\Gamma\|S_0\rangle\\&\quad=\omega_{xS_f}\sum_{ij\Gamma}(-1)^{S_0-S_f-\Gamma-\lambda_i}(2\Gamma+1)^{1/2}W(\lambda_i\lambda_j S_0 S_0;\Gamma S_f)\langle S_0\|\{[\hat{\bar{O}}_{y\lambda_i},\hat{O}^\dagger_{x\lambda_j}]\}^\Gamma\|S_0\rangle.\end{aligned} \tag{7}$$

The quantity W in these equations is a Racah coefficient, $\hat{\bar{O}}_{y\lambda_i}$ is the tensor operator corresponding to the Hermitian adjoint of $\hat{O}^\dagger_{y\lambda_i}$,[27] ω_{xS_f} is the excitation energy from $|S_0\rangle\rangle$ to $|xS_f\rangle\rangle$, and the sums over i and j are sums over all tensor operators with different ranks λ_i and λ_j, as in Eq. (3). The only difference amongst the three TEOMs in Eqs. (5)–(7) comes in the reduced matrix elements, $\langle S_0\|\{\cdots\}^\Gamma\|S_0\rangle$.

In order to derive Eq. (6) from Eq. (5), the so-called "killer condition" [Eq. (2)] must be satisfied. Equation (7) is equivalent to Eq. (6) only if $|S_0\rangle\rangle$ is an eigenfunction of the Hamiltonian $\hat{H}$. Amongst these three TEOMs, Eq. (7) has the favorable features that the double commutator in the reduced matrix elements has lower rank as compared to the first formulation in Eq. (5) and furthermore that both sides of the Eq. (7) are Hermitian.[27] If the killer condition is not satisfied, however, then the use of either Eq. (6) or Eq. (7) may be problematic, as discussed below.

C. Spin-adapted, spin-flip CIS

In this work, the excitation operators involved in the TEOMs are truncated at the single excitation level. In other words, we only focus on removing the spin contamination in traditional (spin-incomplete) spin-flip CIS and its time-dependent Hartree-Fock (TD-HF) extension. Higher-order excitation operators could, in principle, be included to introduce additional electron correlation.

Single excitation operators can be grouped into two kinds of tensors, one having rank zero (singlet coupling) and the other having rank one (triplet coupling).[34] Meanwhile, Eqs. (5)–(7) require the following triangle relations to be fulfilled:

$$|S_0 - S_f| \le \lambda_i \le |S_0 + S_f|, \tag{8a}$$

$$|S_0 - S_f| \le \lambda_j \le |S_0 + S_f|, \tag{8b}$$

$$|\lambda_i - \lambda_j| \le \Gamma \le |\lambda_i + \lambda_j|, \tag{8c}$$

$$|S_0 - S_0| \le \Gamma \le |S_0 + S_0|. \tag{8d}$$

In spin-flip methods, we usually look for the excited states whose total spin angular momentum is one unit smaller than that of the reference state, $S_f = S_0 - 1$. Thus, only triplet-coupled single excitation operators (i.e., $\lambda_i = \lambda_j = 1$) satisfy the above triangle relations. These tensor operators have the following components when represented in the molecular orbital (MO) basis:

$$\hat{O}^\dagger_{pq}(1,1) = -\hat{a}^\dagger_p \hat{a}_{\bar{q}}, \tag{9a}$$

$$\hat{O}^\dagger_{pq}(1,0) = \frac{1}{\sqrt{2}}(\hat{a}^\dagger_p \hat{a}_q - \hat{a}^\dagger_{\bar{p}} \hat{a}_{\bar{q}}), \tag{9b}$$

$$\hat{O}^\dagger_{pq}(1,-1) = \hat{a}^\dagger_{\bar{p}} \hat{a}_q, \tag{9c}$$

where $\hat{a}^\dagger_p$ creates an α-spin electron in orbital ϕ_p and $\hat{a}_{\bar{q}}$ annihilates a β-spin electron in orbital ϕ_q.

Previous work by Li and Liu uses Eq. (7) as the working equation.[24–26] However, in the SF-CIS case, the killer condition in Eq. (2) is not satisfied for excitations within the open-shell space, and as a result both Eqs. (6) and (7) will generate spurious solutions. The reason is that the excitation space is overcomplete, but Eqs. (6) and (7) are not capable of removing this overcompleteness. Consequently, we choose Eq. (5) as our working equation, and we will show that this equation automatically removes the overcompleteness of the excitation space, by symmetry.

An alternative way to solve this problem is to introduce an operator that projects out the reference state, so that the killer condition is fulfilled by construction. This procedure has been shown to be successful in scalar equation-of-motion calculations.[35] We can also extend this approach to TEOMs, simply by writing the tensor operators in Eqs. (1) and (2) with the following general forms:

$$\hat{O}^\dagger_{x\lambda} = \sum_i (-1)^{S_f-\lambda_i}\left(\frac{2S_f+1}{2\lambda_i+1}\right)^{1/2}\left\{\{O^\dagger_{x\lambda_i}|S_0\rangle\rangle\}^{S_f}\langle\langle S_0|\right\}^{\lambda_i}, \tag{10a}$$

$$\hat{O}_{x\lambda} = \sum_i (-1)^{S_f-\lambda_i}\left(\frac{2S_f+1}{2\lambda_i+1}\right)^{1/2}\left\{|S_0\rangle\rangle\{\langle\langle S_0|O_{x\lambda_i}\}^{S_f}\right\}^{\lambda_i}. \tag{10b}$$

Given these two tensor operators, the killer condition [Eq. (2)] is always satisfied, and the three TEOMs in Eqs. (5)–(7) become formally equivalent if $|S_0\rangle\rangle$ is an eigenfunction of the Hamiltonian. This is not, however, the approach that is pursued here.

Now we can express the TEOM in Eq. (5) using the spin-tensor basis shown in Eq. (9). This results in the following matrix representation of the TEOM:

$$\mathbf{MZ}(x) = \omega_x \mathbf{NZ}(x), \tag{11}$$

where the matrix elements of **M** and **N** are

$$M_{pq,rs} = \sum_\Gamma (-1)^{S_0-S_f-\Gamma-1}(2\Gamma+1)^{1/2}W(11S_0S_0;\Gamma S_f) \times \langle S_0\|\{\hat{\bar{O}}_{pq}(1)\times[\hat{H},\hat{O}^\dagger_{rs}(1)]\}^\Gamma\|S_0\rangle, \tag{12}$$

$$N_{pq,rs} = \sum_\Gamma (-1)^{S_0-S_f-\Gamma-1}(2\Gamma+1)^{1/2}W(11S_0S_0;\Gamma S_f) \times \langle S_0\|\{\hat{\bar{O}}_{pq}(1)\times\hat{O}^\dagger_{rs}(1)\}^\Gamma\|S_0\rangle. \tag{13}$$

The reduced matrix elements in Eqs. (12) and (13) can be evaluated using the Wigner-Eckart theorem,

$$\langle\Gamma\|\hat{O}(\lambda)\|\Gamma_1\rangle = \frac{\sqrt{2\Gamma+1}}{C(\Gamma_1\mu_1\lambda\nu;\Gamma\mu)}\langle\Gamma\mu|\hat{O}(\lambda,\nu)|\Gamma_1\mu_1\rangle, \tag{14}$$

where C is a Clebsch-Gordan coefficient, $|\Gamma\mu\rangle$ denotes an angular momentum eigenstate whose total angular momentum is Γ and whose z-component is μ, and $\langle\Gamma\|\hat{O}(\lambda)\|\Gamma_1\rangle$ is the reduced matrix element. Using Eq. (14), the reduced matrix elements in **M** can be expressed as

$$\langle S_0\|\{\hat{\bar{O}}_{pq}(1)\times[\hat{H},\hat{O}^\dagger_{rs}(1)]\}^\Gamma\|S_0\rangle = \frac{(2\Gamma+1)^{1/2}\langle S_0S_0|\{\hat{\bar{O}}_{pq}(1)\times[\hat{H},\hat{O}^\dagger_{rs}(1)]\}^\Gamma_0|S_0S_0\rangle}{C(S_0S_0\Gamma0;S_0S_0)}. \tag{15}$$

In the notation $|S_0S_0\rangle$, the first S_0 is the total spin quantum number and the second S_0 represents the quantum number for the z-component of the spin vector, which makes $|S_0S_0\rangle$ a high-spin state. In Eq. (15), we use the normal spin-flip convention wherein the high-spin open-shell state $|S_0S_0\rangle$ is taken to be the reference state.

The numerator of the right side of Eq. (15), which is a coupled product between excitation operators, can be derived readily:

$$\langle S_0S_0|\{\hat{\bar{O}}_{pq}(1)\times[\hat{H},\hat{O}^{\dagger}_{rs}(1)]\}^{\Gamma}_{0}|S_0S_0\rangle = \sum_{\mu}\langle S_0S_0|\hat{\bar{O}}_{pq}(1,-\mu)\times[\hat{H},\hat{O}^{\dagger}_{rs}(1,\mu)]|S_0S_0\rangle \times C(1(-\mu)1\mu;\Gamma 0). \tag{16}$$

The quantity $\hat{\bar{O}}_{pq}(1,-\mu)$ is defined as[27]

$$\hat{\bar{O}}_{pq}(1,-\mu) = (-1)^{1-\mu}\hat{O}_{pq}(1,\mu). \tag{17}$$

Finally, the matrix elements of **M** can be evaluated. The results are very similar to those derived by Li and Liu,[24] based on the TEOM in Eq. (7), and the details are relegated to the Appendix. The matrix elements of **N** can be derived in the same way, nevertheless it is worth demonstrating the structure of **N**, since this is what guarantees that the overcompleteness of the excitation space is removed automatically. We next proceed to demonstrate this structure.

For SA-SF-CIS, we choose p and q in Eq. (9) to run over all MOs. Namely, $\hat{O}^{\dagger}(1)$ is expanded in the following way if we neglect the redundant excitations:

$$\hat{O}^{\dagger}(1) = \sum_{ai}\hat{O}^{\dagger}_{ai}(1)X^{\mathrm{CV}}_{ai} + \sum_{ui}\hat{O}^{\dagger}_{ui}(1)X^{\mathrm{CO}}_{ui} + \sum_{au}\hat{O}^{\dagger}_{au}(1)X^{\mathrm{OV}}_{au} + \sum_{tu}\hat{O}^{\dagger}_{tu}(1)X^{\mathrm{OO}}_{tu} + \sum_{ia}\hat{O}^{\dagger}_{ia}(1)Y^{\mathrm{VC}}_{ia} + \sum_{iu}\hat{O}^{\dagger}_{iu}(1)Y^{\mathrm{OC}}_{iu} + \sum_{ua}\hat{O}^{\dagger}_{ua}(1)Y^{\mathrm{VO}}_{ua}. \tag{18}$$

In Eq. (18), we use **X** and **Y** to represent the excitation and de-excitation parts of the amplitude, respectively. Superscripts on the quantities X_{pq} and Y_{qp} indicate the excitation type, e.g., X^{CV}_{ai} is the coefficient for excitation of one electron from a closed-shell, doubly occupied MO ϕ_i and into a virtual MO ϕ_a. Using the spin-tensor basis above, the matrix **N** can be expressed explicitly as $\mathbf{N} = \mathbf{N_{XX}} \oplus \mathbf{N_{YY}}$ where

$$\mathbf{N_{XX}} = \begin{pmatrix} \delta_{ij}\delta_{ab} & 0 & 0 & 0 \\ 0 & \left(\frac{2S_0+1}{2S_0}\right)\delta_{ij}\delta_{uv} & 0 & 0 \\ 0 & 0 & \left(\frac{2S_0+1}{2S_0}\right)\delta_{uv}\delta_{ab} & 0 \\ 0 & 0 & 0 & \mathbf{N}^{\mathbf{OO\text{-}OO}} \end{pmatrix}, \tag{19}$$

and $\mathbf{N_{YY}} = \mathbf{0}$. The block $\mathbf{N}^{\mathbf{OO\text{-}OO}}$ is the only part of $\mathbf{N_{XX}}$ that is not diagonal. This block is singular, with matrix elements

$$N^{\mathrm{OO\text{-}OO}}_{tu,vw} = -\left(\frac{2S_0+1}{2S_0(2S_0-1)}\right)\delta_{tu}\delta_{vw} + \left(\frac{2S_0+1}{2S_0-1}\right)\delta_{tv}\delta_{uw}. \tag{20}$$

The rank of $\mathbf{N}^{\mathbf{OO\text{-}OO}}$ is less than its dimension, which removes the overcompleteness of the OO excitation space. For example, if $S_0 = 1$ and $S_f = 0$ (singlet states from a high-spin triplet reference), then $\mathbf{N}^{\mathbf{OO\text{-}OO}}$ can be expressed as

$$\mathbf{N}^{\mathbf{OO\text{-}OO}}_{S_0=1} = \begin{pmatrix} \frac{3}{2} & 0 & 0 & -\frac{3}{2} \\ 0 & 3 & 0 & 0 \\ 0 & 0 & 3 & 0 \\ -\frac{3}{2} & 0 & 0 & \frac{3}{2} \end{pmatrix}, \tag{21}$$

which has a rank of 3. It is easy to show that all possible single spin-flipping excitations within the open-shell space from a high-spin triplet reference state will generate three singlet states and one triplet state. The fact that the matrix in Eq. (21) has rank 3 rather than 4 guarantees that the one triplet state is excluded from the solutions. At this point, we have proved that by using Eq. (5) as the working equation for SA-SF-CIS, all the solutions will have the correct spin eigenvalue and no spurious solutions will be generated.

It is also interesting to note that the de-excitation part of the TEOM vanishes, i.e., $\mathbf{N_{YY}} = \mathbf{0}$. As such, there is no concept of a "Tamm-Dancoff approximation,"[36] since $\mathbf{Y} \equiv \mathbf{0}$, and the SA-SF-CIS method derived here reduces to the spin-complete SF-CIS method of Sherrill and co-workers.[28] The benefit of our TEOM-based derivation is that we do not have to add more electron configurations into the CI equations, as was done in Ref. 28. Actually, the matrix dimensions of **M** and **N** in SA-SF-CIS are exactly the same as those in (spin-incomplete) SF-CIS, due to the spin-tensor basis that is used here. In other words, the spin contamination in SF-CIS can be removed without additional computational cost by applying the TEOM approach.

D. DFT correction

In principle, the current SA-SF-CIS method can be extended to its corresponding DFT counterpart by introducing a Hamiltonian $\hat{H}^{\mathrm{DFT}}$ associated to density functional theory. This Hamiltonian is required to generate the exact ground-state energy from the single-determinant reference state,

$E_0^{\text{exact}} = \langle S_0|\hat{H}^{\text{DFT}}|S_0\rangle$. Unfortunately, no such Hamiltonian is known in analytic form. Instead, we propose an empirical correction to the matrix elements in the SA-SF-CIS working equation to capture dynamical correlation using a density functional. The motivation behind this *ad hoc* correction is similar in spirit to the idea that underlies the DFT/MRCI method.[31,32] We will denote our method as SA-SF-DFT.

In DFT/MRCI, the major correction from DFT is added to the diagonal matrix elements of the MRCI Hamiltonian in the following way. Using singly-excited Slater determinants $|\Phi_{pq}\rangle$ rather than configuration state-functions as the basis, we have

$$\langle\Phi_{pq}|\hat{H}^{\text{DFT}} - E_0^{\text{DFT}}|\Phi_{pq}\rangle = F_{pp}^{\text{KS}} - F_{qq}^{\text{KS}} + \langle pq||qp\rangle + p_J\langle pq|pq\rangle - p(N_o)\langle pq|qp\rangle. \tag{22}$$

Here, $|\Phi_{pq}\rangle$ indicates $q \rightarrow p$ excitation, E_0^{DFT} is the ground-state DFT energy, $\mathbf{F}^{\text{KS}}$ is the Kohn-Sham Fock matrix, p_J is a fitting parameter, and $p(N_o)$ is an empirical function depending on the number of open shells, N_o. The quantities p_J and $p(N_o)$ are optimized for each density functional, and for the BH&HLYP functional,[37] good performance is obtained for $p_J = 1 - C_{\text{HF}} = 0.5$. (Re-parameterization is required for the functionals having a substantially different fraction of Hartree-Fock exchange.[32])

Since the correction from $\langle pq|pq\rangle$ is usually larger than that from $\langle pq|qp\rangle$, we will neglect the final term in Eq. (22) in our method. Moreover, we set $p_J = 1 - C_{\text{HF}}$ and apply the correction to all matrix elements including off-diagonal terms, for simplicity. The matrix elements in SA-SF-DFT therefore have the following form:

$$\langle\Phi_{pq}|\hat{H}^{\text{DFT}} - E_0^{\text{DFT}}|\Phi_{rs}\rangle = \delta_{qs}F_{pr}^{\text{KS}} - \delta_{pr}F_{qs}^{\text{KS}} + \langle ps||qr\rangle + (1 - C_{\text{HF}})\langle ps|rq\rangle. \tag{23}$$

This is precisely the same matrix element as in collinear SF-TDDFT,[1] which provides some justification for the generally good performance of that method. In principle, we could tune the value of p_J in collinear SF-TDDFT for any density functional, in an effort to obtain accurate energetics. As such, the requirement of ≈50% Hartree-Fock exchange for good results in collinear SF-TDDFT, which was discovered empirically in Ref. 1, may actually depend upon how we "translate" the CI method to TDDFT and may have less to do with spin contamination, as was suggested in Ref. 24. Additional evidence in support of this argument comes from non-collinear SF-TDDFT, which usually performs well with less Hartree-Fock exchange,[5,11] despite the fact that it is also spin contaminated. This is mainly because the CI method and TDDFT are connected in a different way, namely, through non-collinear kernels, and the parameterization approach for non-collinear SF-TDDFT is distinct from that for collinear SF-TDDFT.

Besides the simple form of Eq. (23), there is another advantage to calculating the matrix elements in this way. The Wigner-Eckart theorem is used in deriving the TEOMs, and this theorem assumes that the components of a spin tensor are energetically degenerate because the Hamiltonian of the system is spin-independent. This degeneracy is satisfied only if we use the same Hamiltonian to calculate the ground-state energy and the matrix elements in the TEOM. Equation (23), based on a restricted open-shell Hartree-Fock[38] (ROHF) reference state, satisfies the spin-degeneracy condition[24] and thus partly removes the ambiguity associated with application of the Wigner-Eckart theorem. Some ambiguity remains, insofar as the Kohn-Sham Fock matrix that is used in Eq. (23) is calculated from a different Hamiltonian as compared to $\hat{H}^{\text{DFT}}$.

Although, in principle, it would be possible to use non-collinear exchange-correlation (XC) functionals to add a DFT correction to SA-SF-CIS, we will use collinear functionals exclusively. The reason is that the ROHF reference state exactly satisfies the degeneracy condition amongst the various components of a spin multiplet, and the form of the collinear matrix elements [Eq. (23)] does not alter this fact. For non-collinear functionals, the form of the **K** matrices introduced in the Appendix is altered in a way that may not respect the spin-degeneracy condition.[24] (Li and Liu[24] suggest how empirical parameters could be introduced to partially restore this degeneracy, but we will not attempt this here.)

Note that the use of Eq. (23) in conjunction with a spin-complete formalism does engender some double-counting of electron correlation. The same can be said of DFT/MRCI, and in that method the off-diagonal matrix elements are modified in an attempt to counterbalance some of this double-counting.[32] Similar modifications may help the SA-SF-DFT method, but we have not pursued these yet. It should be noted that collinear SF-TDDFT itself is already subject to some double-counting.

III. NUMERICAL EXAMPLES

The SA-SF-DFT method has been implemented in a locally modified version of the Q-Chem program,[39] and in this section we evaluate its performance. All calculations were performed using Q-Chem except for some benchmark MRCI calculations, which were performed using the Orca program.[40] The examples that we consider here involve singlet excitations starting from a high-spin ROHF reference state[38] for the triplet. It should be noted that the formalism is more general than triplet-to-singlet spin-flipping transitions, however. The spin states S_0 and S_f (Section II) can be any integer or half-integer values, subject to the constraint that $S_f = S_0 - 1$.

A. Ethylene torsion

Ethylene torsion is a prototypical example for testing how electronic structure methods describe biradicals. Collinear SF-TDDFT performs well for this system,[1] whereas most spin-conserving, single-reference methods (e.g., TDDFT or EOM-CCSD) fail to yield smooth potential curves at the D_{2d} geometry,[29] because the ground and excited states are described in an unbalanced manner.

Here, we study potential energy curves along the double-bond twisting coordinate of the singlet N, V, and Z states. We compare collinear SF-TDDFT, SA-SF-DFT, and SA-SF-CIS potential energy curves to those obtained at the MRCI singles and doubles level. The BH&HLYP functional[37] is used for the

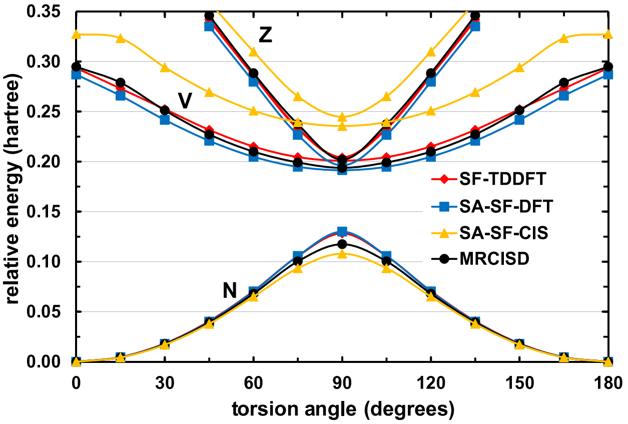

FIG. 2. Potential energy curves along the double-bond torsion coordinate of ethylene, for the singlet states N, V, and Z. The SF-TDDFT results use the collinear formalism and note that SA-SF-CIS (without the *ad hoc* DFT correction) is equivalent to the spin-complete SF-CIS method of Ref. 28. The zero in energy corresponds to the singlet ground state at its equilibrium geometry.

DFT calculations, and a CAS(2,2) singlet ground state is used as the reference state for the MRCI calculations. Potential scans along the torsion coordinate use the cc-pVTZ basis set starting from the equilibrium geometry optimized at the ωB97X-D/6-31G* level. Potential scans are plotted in Fig. 2.

All four of the aforementioned methods are in good agreement with each other for the N state, except that the two DFT methods slightly overestimate the barrier height and SA-SF-CIS slightly underestimates it, as compared to the MRCI result. For the V and Z states, potential curves computed using the two DFT methods exhibit quantitative agreement with MRCI results, whereas the excitation energies predicted by SA-SF-CIS are more than 1 eV too large at the D_{2d} geometry. This is undoubtedly due in large part to the lack of dynamical correlation in this approach, and the same effect was seen recently in time-dependent projected Hartree Fock calculations of twisted ethylene.[29] Nevertheless, each of the methods examined here produces a smooth potential curve and at least quasi-degeneracy between the V and Z states at the D_{2d} geometry. This is because all three spin-flip approaches (and MRCI as well) treat the ground and excited states in a balanced manner and include the most important double excitations.

Note also that there is essentially no difference between SA-SF-DFT and collinear SF-TDDFT results for the ethylene torsion problem. This is not surprising given that the latter approach exhibits nearly zero spin contamination for the electronic states in question. Recalling that we construct the matrix elements of SA-SF-DFT in the same way as in collinear SF-TDDFT [Eq. (23)], these two methods become identical in cases where SF-TDDFT exhibits no spin contamination.

B. Vertical excitation energies of nucleobases

Previous collinear SF-TDDFT studies have shown that this method tends to overestimate vertical excitation energies for nucleobases,[18] and it is interesting to examine whether SA-SF-DFT can correct this problem. Equilibrium structures of the nucleobases were optimized at the B3LYP/6-311G(2df,2pd) level, and then SA-SF-DFT and collinear SF-TDDFT excitation energies were computed at the BH&HLYP/aug-cc-pVTZ level.

TABLE I. Vertical excitation energies (in eV) for the lowest two singlet excited states of the five nucleobases. For collinear SF-TDDFT, the value of $\langle \hat{S}^2 \rangle$ is given in parentheses, in units of $\hbar^2$.

	SA-SF-DFT		Collinear SF-TDDFT		Benchmark	
Nucleobase	S_1	S_2	S_1	S_2	S_1	S_2
Uracil	5.35	5.56	5.50 (1.09)	5.80 (0.16)	5.00[a]	5.25[a]
Adenine	5.24	5.28	4.79 (1.09)	5.31 (1.11)	5.13[b]	5.20[b]
Thymine	5.21	5.66	5.60 (1.08)	5.66 (0.16)	5.14[c]	5.60[c]
Cytosine	4.74	5.60	5.28 (0.29)	5.45 (1.04)	4.76[d]	5.24[d]
Guanine	5.02	5.18	4.95 (1.04)	5.02 (1.05)	4.76[b]	5.09[b]
MAE[e]	0.16	0.18	0.40	0.20		

[a] CR-EOM-CCSD(T)/aug-cc-pVTZ results from Ref. 41.
[b] CAS(10,10)PT2/ANO-double-ζ results from Ref. 42.
[c] EOM-CCSD/TZVP results from Ref. 43.
[d] CR-EOM-CCSD(T)/cc-pVDZ results from Ref. 44.
[e] Mean absolute error with respect to the benchmarks.

Table I summarizes the vertical excitation energies of the lowest two singlet excited states for all five nucleobases, along with benchmark results from correlated wavefunction calculations. For the collinear SF-TDDFT calculations, values of $\langle \hat{S}^2 \rangle$ are listed as well. Since most of the states in the collinear SF-TDDFT calculations are heavily spin-contaminated, with $\langle \hat{S}^2 \rangle \approx 1$ (in units of $\hbar^2$), we assign those states with $\langle \hat{S}^2 \rangle < 1.5$ to be singlet states.

We observe that SA-SF-DFT affords reasonable excitation energies for the S_1 and S_2 states of all five nucleobases, with a mean absolute error (MAE) 0.17 eV. For the S_1 state, collinear SF-TDDFT affords a large MAE (0.40 eV), although the MAE for the S_2 state is comparable at 0.20 eV. It is possible that the reasonable performance of the heavily spin-contaminated SF-TDDFT calculations is accidental, since averaging over the triplet and singlet states sometimes results in good excitation energies in unrestricted TDDFT calculations for open-shell systems,[26] and many of the ostensibly singlet excitations computed using SF-TDDFT in Table I are better described as roughly equal mixtures of singlet and triplet.

Considering the similarity of the matrix elements in DFT/MRCI [Eq. (22)] and collinear SA-SF-DFT [Eq. (23)], one might anticipate comparable performance given an appropriate reference state. [For example, a high-spin triplet reference state in SA-SF-DFT corresponds to a CAS(2,2) reference state in MRCI.] On the other hand, the traditional, collinear SF-TDDFT approach with the same functional (e.g., BH&HLYP) usually shows much worse performance, especially near the Franck-Condon region. From the examples in Sections III A and III B, we may conclude that the poor performance of collinear SF-TDDFT is mostly caused by the spin contamination, while an XC functional with ≈50% Hartree-Fock exchange should still be a reasonable choice for collinear SF-TDDFT.

In a previous study of the nucleobases using range-separated hybrid functionals with non-empirical tuning, a MAE of 0.19 eV for the $S_0 \rightarrow S_1$ excitations was reported.[45]

This further suggests that the performance of SA-SF-DFT is perhaps about the best that one can expect from contemporary TDDFT. Based on these few, simple tests, we can say that the correction to excitation energies that is obtained by removing the spin contamination in collinear SF-TDDFT is sizable, and SA-SF-DFT seems like a promising method.

C. State assignment in SF-TDDFT

Although there are a few examples of *ab initio* MD simulations using SF-TDDFT,[12,20,21] and other examples of using SF-TDDFT to locate minimum-energy crossing points (MECPs) along conical seams,[10,13,14,16,18] the spin contamination problem makes it challenging to assign the excited states correctly and consistently across the potential energy surface. Here, we demonstrate this problem with numerical examples.

1. *Nonadiabatic ab initio MD*

We carried out a fewest-switches surface hopping simulation[46] of uracil, using collinear SF-TDDFT at the BH&HLYP/6-31G* level. Three successive snapshots along one trajectory, spanning only 1 fs of simulation time, serve to demonstrate the state assignment problem; excitation energies and $\langle \hat{S}^2 \rangle$ values for these snapshots are given in Table II. Within the time window presented in the table, the S_1 and T_1 states change their order, but this can be difficult to detect in the heavily spin-contaminated SF-TDDFT calculations. The consequence of an incorrect state assignment in an *ab initio* MD simulation (or excited-state geometry optimization, for that matter) might be energy jumps, propagation on the wrong state, and other nonsense ultimately leading to incorrect relaxation times and branching ratios, or even convergence failure. As such, an effective state-tracking algorithm is required whenever SF-TDDFT is used to move about an excited-state potential energy surface.

A straightforward way to do this, which we have sometimes found to be effective, is to monitor the change in the excited-state transition density. Within the Tamm-Dancoff approximation, this quantity is

$$T(\mathbf{r},\mathbf{r}') = \sum_{ai} X_{ai}\, \phi_i(\mathbf{r})\, \phi_a(\mathbf{r}'). \tag{24}$$

Let us denote the transition density at a subsequent geometry as

$$\widetilde{T}(\mathbf{r},\mathbf{r}') = \sum_{bj} \widetilde{X}_{bj}\, \widetilde{\phi}_j(\mathbf{r})\, \widetilde{\phi}_b(\mathbf{r}'). \tag{25}$$

We wish to examine the overlap integral

$$\begin{aligned}\int d\mathbf{r}\, d\mathbf{r}'\, T(\mathbf{r},\mathbf{r}')\, \widetilde{T}(\mathbf{r}',\mathbf{r}) &= \sum_{ijab} X_{ai}\widetilde{X}_{bj} \langle \phi_i | \widetilde{\phi}_j \rangle \langle \phi_a | \widetilde{\phi}_b \rangle \\ &= \mathrm{tr}(\mathbf{X}\mathbf{C}^\dagger\mathbf{S}\widetilde{\mathbf{C}}\widetilde{\mathbf{X}}^\dagger\widetilde{\mathbf{C}}^\dagger\mathbf{S}^\dagger\mathbf{C}),\end{aligned} \tag{26}$$

where $S_{\mu\nu} = \langle \mu | \widetilde{\nu} \rangle$ is the overlap between the atomic orbitals at the two different geometries. Based on the overlaps between various transition densities and the assumption that it is possible to assign spin multiplicities to the SF-TDDFT states at the Franck-Condon geometry, one may hope to track those multiplicities as the geometry and excited states evolve in time.

TABLE II. Excitation energies for three sequential time steps of a surface-hopping simulation of gas-phase uracil performed at the BH&HLYP/6-31G* level.

	SA-SF-DFT/RPA		Collinear SF-TDDFT			SF-RASCI	
Time/fs	State	ω/eV	State	ω/eV	$\langle \hat{S}^2 \rangle/\hbar^2$	State	ω/eV
26.6	S_1	2.36	S_1	2.05	1.18	S_1	2.39
			T_1	2.19	1.81		
	S_2	3.82	S_2	3.66	0.63	S_2	3.85
27.1			T_1	2.12	1.52		
	S_1	2.37	S_1	2.20	1.51	S_1	2.44
	S_2	3.83	S_2	3.72	0.66	S_2	3.90
27.6			T_1	2.14	1.91		
	S_1	2.39	S_1	2.24	1.15	S_1	2.47
	S_2	3.82	S_2	3.76	0.65	S_2	3.93

The aforementioned state-tracking procedure was used to assign multiplicities to the SF-TDDFT calculations reported in Table II. Note that if the assignment were based solely on the value of $\langle \hat{S}^2 \rangle$, e.g., with states having $\langle \hat{S}^2 \rangle > 1.5$ assigned as triplets, then at $t = 27.1$ fs we would assign as S_1 the state that is actually labeled as S_2 in Table II. This illustrates the extent to which $\langle \hat{S}^2 \rangle$ completely fails as a reliable quantum number in SF-TDDFT, which in our experience is quite common away from the Franck-Condon region.[18]

On the other hand, the state-tracking procedure suggested in Eq. (26) is not guaranteed to work, especially in nonadiabatic MD simulations. Each spin-contaminated state in SF-TDDFT is a mixture of different spin multiplicities, and when the two states with different multiplicities (singlet and triplet in the present example) become nearly degenerate, their wavefunctions usually vary smoothly with respect to nuclear geometry. This is analogous to an avoided crossing between two strongly coupled states, and state-tracking algorithms can easily fail to identify a change in the ordering of two states with different multiplicities. As such, the most reliable way to solve the state assignment problem is to use spin-adapted methods.

Table II also lists SA-SF-DFT excitation energies for uracil along with benchmarks computed at the level of spin-flip restricted active space configuration interaction (SF-RASCI).[47] We computed these benchmarks using a large active space [RAS(2,10)-SF] to ensure accuracy, and we find that they agree very well with SA-SF-DFT calculations. This demonstrates that the SA-SF-DFT approach not only cures the state assignment problem but also improves upon collinear SF-TDDFT energetics. As such, SA-SF-DFT appears to be a promising method for nonadiabatic *ab initio* MD simulations.

2. *Optimization of MECPs*

As another example to demonstrate the state assignment problem in SF-TDDFT, we searched for the MECP along

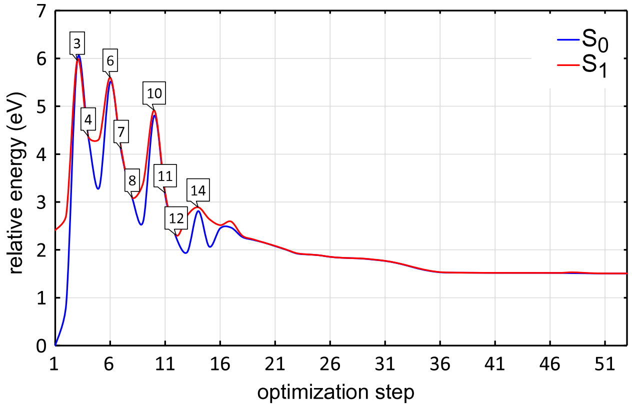

FIG. 3. Potential energy curves along the S_0/S_1 MECP optimization trajectory of ethylene, calculated using collinear SF-TDDFT (BH&HLYP/6-31G* level). Labels above the curves show at which steps the state assignment problem appears. The zero of energy is the ground state at the D_{2d} geometry.

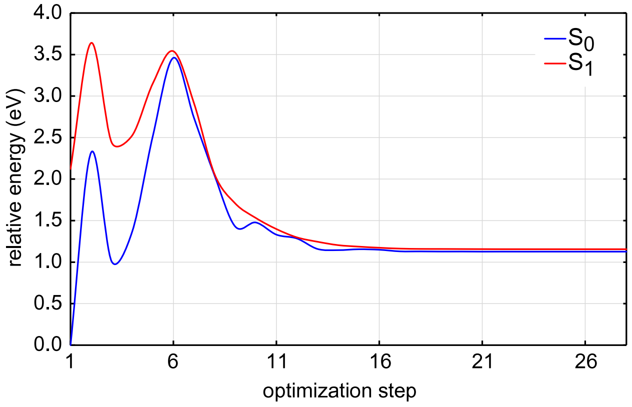

FIG. 4. Potential energy curves along the S_0/S_1 MECP optimization trajectory of ethylene, calculated using SA-SF-DFT (BH&HLYP/6-31G* level). The zero of energy is the ground state at the D_{2d} geometry.

the crossing seam between the S_0 and S_1 states of ethylene, using both SF-TDDFT and SA-SF-DFT. The D_{2d} geometry served as the starting point in both calculations, and for SF-TDDFT, we assign the states using $\langle \hat{S}^2 \rangle$ alone, with any state having $\langle \hat{S}^2 \rangle < 1.2$ assigned as a singlet. We do not yet have analytic energy gradients for the SA-SF-DFT method, so for this method the gradients are evaluated by finite difference, and we use a penalty-constrained algorithm[48] to locate the MECP. This algorithm does not require derivative couplings. For the SF-TDDFT calculations, both analytic gradients and analytic derivative couplings are available,[9] and we can use a MECP optimization algorithm that takes advantage of both.[49]

Figure 3 plots the energies of the two states involved in the MECP optimization, at the SF-TDDFT level. Optimization steps at which the state assignment is ambiguous are labeled, and in Table III we provide the $\langle \hat{S}^2 \rangle$ values of the lowest three states at each optimization step. For the first 14 optimization steps, the S_0 state and the low-lying triplet state are nearly degenerate and strongly coupled with each other, which makes state assignments very difficult. For example, whereas in the second step we can assign state 1 as S_0 and state 3 as S_1 without ambiguity, the use of $\langle \hat{S}^2 \rangle$ in the third step would assign state 1 as S_0 and state 2 as S_1, but by examining the orbitals and CI coefficients we found that state 2 and state 3 are the true S_0 and S_1 states, whereas state 1 is a triplet. As a result of this incorrect state assignment, the efficiency of MECP optimization is greatly reduced, which can be inferred from the steep peaks in Fig. 3 that occur precisely in regions where the state assignment is ambiguous. Since the states are assigned incorrectly, the energy gradients and derivative couplings are calculated for the wrong states, and it takes 18 steps to reach the correct intersection seam.

TABLE III. Values of $\langle \hat{S}^2 \rangle$ (in units of $\hbar^2$) for the lowest three states of ethylene in the first 19 optimization steps shown in Fig. 3.

	Values of $\langle \hat{S}^2 \rangle$		
Step	State 1	State 2	State 3
1	0.01	2.01	0.06
2	0.02	2.00	0.05
3	1.14	0.90	0.02
4	1.10	0.95	0.02
5	0.07	1.97	0.03
6	0.90	1.18	0.03
7	0.93	1.15	0.05
8	1.00	1.05	0.06
9	0.75	1.30	0.05
10	1.03	1.06	0.04
11	0.93	1.14	0.06
12	0.99	1.06	0.08
13	1.61	0.43	0.09
14	1.20	0.85	0.09
15	0.29	1.76	0.08
16	0.27	1.81	0.05
17	0.12	2.01	0.02
18	2.00	0.10	0.04
19	2.00	0.03	0.10

Although a state-tracking algorithm, such as that discussed above, might improve the performance of SF-TDDFT for MECP optimization, the SA-SF-DFT method is a better solution. Energies along the S_0/S_1 MECP optimization computed using the latter method are plotted in Fig. 4. In this case, the energy variations along the optimization pathway are much smaller and the optimization reaches the correct intersection seam within 6 steps and finally converges to the MECP in fewer steps than the SF-TDDFT calculation, despite the fact that the latter calculation is able to exploit analytic derivative couplings. (MECP optimizations using SF-TDDFT *without* analytic derivative couplings require even more steps.[9])

IV. SUMMARY

We have derived and implemented the spin-adapted counterpart of conventional collinear SF-TDDFT, which we denote as SA-SF-DFT. The underlying SA-SF-CIS method is equivalent to a previous spin-complete implementation of SF-CIS[28] but is derived here based on an equation-of-motion formulation in a spin-tensor basis. Our derivation results in matrices of similar dimension as those in SF-TDDFT, meaning that the cost of the CI-like part of the SA-SF-CIS calculation is not significantly increased by the extension to spin eigenstates. To this SA-SF-CIS foundation, we then add an *ad hoc* density-functional correction in order to incorporate dynamical correlation, and this constitutes what we call the SA-SF-DFT method. Roughly speaking, SA-SF-DFT is a spin-flip restricted active space CI method with a DFT correction similar in spirit to that used in DFT/MRCI. Unsurprisingly, this dynamical correlation correction can easily exceed 1 eV for excitation energies, and we find that the performance of SA-SF-DFT represents a consistent improvement over collinear SF-TDDFT.

In addition, SA-SF-DFT is a potentially much more attractive approach to excited-state *ab initio* MD simulations, as compared to SF-TDDFT. This is because

- it is free of spin contamination, and thus not subject to the state-assignment problem that plagues SF-TDDFT;
- it treats ground and excited states on the same footing and thus affords correct topology at conical intersections, including those that involve the ground state; and
- it is just as computationally efficient as SF-TDDFT.

That said, efficient application to *ab initio* MD will require the development an implementation of analytic energy gradients for the SA-SF-DFT method. Relative to the gradients for traditional SF-TDDFT, this is complicated by the additional orbital subspaces that are necessary for the spin-adapted version (as illustrated in Fig. 1), and thus by additional orbital response terms that will appear in the derivative of Eq. (18). These extra terms should, however, only increase the cost relative to SF-TDDFT by a prefactor that is independent of system size and thus will not increase the formal computational scaling with system size relative to TDDFT or SF-TDDFT.

ACKNOWLEDGMENTS

This work was supported by the National Science Foundation (Grant No. CHE-1300603) and calculations were performed at the Ohio Supercomputer Center under Project No. PAA-0003.[50] J.M.H. is a Camille Dreyfus Teacher-Scholar.

APPENDIX: MATRIX ELEMENTS IN EQ. (12)

In this appendix, we briefly summarize the matrix elements of **M** in Eq. (12), which are derived from Eq. (5) with the spin-tensor basis shown in Eq. (18). More details can be found in Ref. 24.

The matrix **M** is the sum of three matrices,

$$\mathbf{M} = \mathbf{M}^{(0)} - \mathbf{M}^{(1)} + \mathbf{M}^{(2)}, \tag{A1}$$

TABLE IV. Matrix elements of $\mathbf{M}_{+}$, $\mathbf{M}_0$, and $\mathbf{M}_{-}$ not including OO excitations.

Block	Matrix element
CV-CV	$[M_+]_{ai,bj} = \delta_{ij} F^{\alpha}_{ab} - \delta_{ab} F^{\beta}_{ij} + K^{\alpha\beta,\alpha\beta}_{ai,bj}$ $[M_0]_{ai,bj} = \delta_{ij}(F^{\alpha}_{ab} + F^{\beta}_{ab})/2 - \delta_{ab}(F^{\alpha}_{ij} + F^{\beta}_{ij})/2 + K^{t}_{ai,bj}$ $[M_-]_{ai,bj} = \delta_{ij} F^{\beta}_{ab} - \delta_{ab} F^{\alpha}_{ij} + K^{\beta\alpha,\beta\alpha}_{ai,bj}$
CV-CO	$[M_+]_{ai,vj} = \delta_{ij} F^{\alpha}_{av}$ $[M_0]_{ai,vj} = (\delta_{ij} F^{\alpha}_{av} + \delta_{ij} F^{\beta}_{av} - K^{\alpha\alpha,\beta\beta}_{ai,vj} + K^{\beta\beta,\beta\beta}_{ai,vj})/2$ $[M_-]_{ai,vj} = \delta_{ij} F^{\beta}_{av} + K^{\beta\alpha,\beta\alpha}_{ai,vj}$
CO-CV	$[M_+]_{ui,bj} = 0$ $[M_0]_{ui,bj} = (\delta_{ij} F^{\beta}_{bu} - K^{\beta\beta,\alpha\alpha}_{ui,bj} + K^{\beta\beta,\beta\beta}_{ui,bj})/2$ $[M_-]_{ui,bj} = \delta_{ij} F^{\beta}_{bu} + K^{\beta\alpha,\beta\alpha}_{ui,bj}$
CV-OV	$[M_+]_{ai,bv} = -\delta_{ab} F^{\beta}_{iv}$ $[M_0]_{ai,bv} = (-\delta_{ab} F^{\alpha}_{iv} - \delta_{ab} F^{\beta}_{iv} + K^{\alpha\alpha,\alpha\alpha}_{ai,bv} - K^{\beta\beta,\alpha\alpha}_{ai,bv})/2$ $[M_-]_{ai,bv} = -\delta_{ab} F^{\alpha}_{iv} + K^{\beta\alpha,\beta\alpha}_{ai,bv}$
OV-CV	$[M_+]_{au,bj} = 0$ $[M_0]_{au,bj} = (-\delta_{ab} F^{\alpha}_{ju} + K^{\alpha\alpha,\alpha\alpha}_{au,bj} - K^{\alpha\alpha,\beta\beta}_{au,bj})/2$ $[M_-]_{au,bj} = -\delta_{ab} F^{\alpha}_{ju} + K^{\beta\alpha,\beta\alpha}_{au,bj}$
CO-CO	$[M_+]_{ui,vj} = 0$ $[M_0]_{ui,vj} = (\delta_{ij} F^{\beta}_{uv} - \delta_{uv} F^{\beta}_{ij} + K^{\beta\beta,\beta\beta}_{ui,vj})/2$ $[M_-]_{ui,vj} = \delta_{ij} F^{\beta}_{uv} - \delta_{uv} F^{\alpha}_{ij} + K^{\beta\alpha,\beta\alpha}_{ui,vj}$
CO-OV	$[M_+]_{ui,bv} = 0$ $[M_0]_{ui,bv} = -K^{\beta\beta,\alpha\alpha}_{ui,bv}/2$ $[M_-]_{ui,bv} = K^{\beta\alpha,\beta\alpha}_{ui,bv}$
OV-CO	$[M_+]_{au,vj} = 0$ $[M_0]_{au,vj} = -K^{\alpha\alpha,\beta\beta}_{au,vj}/2$ $[M_-]_{au,vj} = K^{\beta\alpha,\beta\alpha}_{au,vj}$
OV-OV	$[M_+]_{au,bv} = 0$ $[M_0]_{au,bv} = (\delta_{uv} F^{\alpha}_{ab} - \delta_{ab} F^{\alpha}_{uv} + K^{\alpha\alpha,\alpha\alpha}_{au,bv})/2$ $[M_-]_{au,bv} = \delta_{uv} F^{\beta}_{ab} - \delta_{ab} F^{\alpha}_{uv} + K^{\beta\alpha,\beta\alpha}_{au,bv}$

where

$$\mathbf{M}^{(0)} = \tfrac{1}{3}(\mathbf{M}_{+} + \mathbf{M}_0 + \mathbf{M}_{-}), \tag{A2}$$

$$\mathbf{M}^{(1)} = \left(\frac{S_0 + 1}{2S_0}\right)(\mathbf{M}_{+} - \mathbf{M}_{-}), \tag{A3}$$

$$\mathbf{M}^{(2)} = \left[\frac{(S_0 + 1)(2S_0 + 3)}{6S_0(2S_0 - 1)}\right](\mathbf{M}_{+} - 2\mathbf{M}_0 + \mathbf{M}_{-}). \tag{A4}$$

The matrix elements of $\mathbf{M}_{+}$, $\mathbf{M}_0$, and $\mathbf{M}_{-}$ are grouped into different blocks. Recall that the blocks associated with de-excitations vanish, which makes the size of **M** about half the size of the orbital rotation Hessian in the conventional time-dependent Hartree-Fock method. Since **M** is not Hermitian, we need to calculate a few more matrix elements as compared to the approach used in Ref. 24. The results are summarized in Tables IV and V. In those tables, **F** is the Fock matrix, and **K** is the coupling matrix defined as

$$K^{\sigma\tau,\sigma'\tau'}_{pq,rs} = \langle p_{\sigma} s_{\tau'} | | q_{\tau} r_{\sigma'} \rangle, \tag{A5}$$

where σ, τ, σ', and τ' denote α or β spin. Finally, $\mathbf{K}^t$ is defined as

$$\mathbf{K}^t = \frac{1}{2}(\mathbf{K}^{\alpha\alpha,\alpha\alpha} + \mathbf{K}^{\beta\beta,\beta\beta} - \mathbf{K}^{\alpha\alpha,\beta\beta} - \mathbf{K}^{\beta\beta,\alpha\alpha}). \tag{A6}$$

TABLE V. Matrix elements of $\mathbf{M}_+$, $\mathbf{M}_0$, and $\mathbf{M}_-$ including OO excitations.

Block	Matrix element
CV-OO	$[M_+]_{ai,vw} = -K^{\alpha\beta,\alpha\beta}_{ai,vw}$ $[M_0]_{ai,vw} = 0$ $[M_-]_{ai,vw} = K^{\beta\alpha,\beta\alpha}_{ai,vw}$
OO-CV	$[M_+]_{tu,bj} = 0$ $[M_0]_{tu,bj} = \delta_{tu}(F^{\alpha}_{bj} - F^{\beta}_{bj})/2$ $[M_-]_{tu,bj} = K^{\beta\alpha,\beta\alpha}_{tu,bj}$
CO-OO	$[M_+]_{ui,vw} = 0$ $[M_0]_{ui,vw} = -\delta_{uv}F^{\beta}_{iw}/2$ $[M_-]_{ui,vw} = -\delta_{uv}F^{\alpha}_{iw} + K^{\beta\alpha,\beta\alpha}_{ui,vw}$
OO-CO	$[M_+]_{tu,vj} = 0$ $[M_0]_{tu,vj} = -\delta_{tu}F^{\beta}_{jv}/2$ $[M_-]_{tu,vj} = -\delta_{tv}F^{\alpha}_{ju} + K^{\beta\alpha,\beta\alpha}_{tu,vj}$
OV-OO	$[M_+]_{au,vw} = 0$ $[M_0]_{au,vw} = \delta_{uw}F^{\alpha}_{av}/2$ $[M_-]_{au,vw} = \delta_{uw}F^{\beta}_{av} + K^{\beta\alpha,\beta\alpha}_{au,vw}$
OO-OV	$[M_+]_{tu,bv} = 0$ $[M_0]_{tu,bv} = \delta_{ut}F^{\alpha}_{bv}/2$ $[M_-]_{tu,bv} = \delta_{uv}F^{\beta}_{bt} + K^{\beta\alpha,\beta\alpha}_{tu,bv}$
OO-OO	$[M_+]_{tu,vw} = 0$ $[M_0]_{tu,vw} = 0$ $[M_-]_{tu,vw} = \delta_{uw}F^{\beta}_{tv} - \delta_{tv}F^{\alpha}_{uw} + K^{\beta\alpha,\beta\alpha}_{tu,vw}$

[1] Y. Shao, M. Head-Gordon, and A. I. Krylov, J. Chem. Phys. **118**, 4807 (2003).

[2] F. Wang and T. Ziegler, J. Chem. Phys. **121**, 12191 (2004).

[3] F. Wang and T. Ziegler, J. Chem. Phys. **122**, 074109 (2005).

[4] K. Yang, R. Peverati, D. G. Truhlar, and R. Valero, J. Chem. Phys. **135**, 044118 (2011).

[5] Y. A. Bernard, Y. Shao, and A. I. Krylov, J. Chem. Phys. **136**, 204103 (2012).

[6] X. Xu, K. R. Yang, and D. G. Truhlar, J. Chem. Theory Comput. **10**, 2070 (2014).

[7] N. Minezawa, Chem. Phys. Lett. **622**, 115 (2015).

[8] X. Zhang and J. M. Herbert, J. Chem. Phys. **142**, 064109 (2015).

[9] X. Zhang and J. M. Herbert, J. Chem. Phys. **141**, 064104 (2014).

[10] N. Minezawa and M. S. Gordon, J. Phys. Chem. A **113**, 12749 (2009).

[11] M. Huix-Rotllant, B. Natarajan, A. Ipatov, C. M. Wawire, T. Deutsch, and M. E. Casida, Phys. Chem. Chem. Phys. **12**, 12811 (2010).

[12] N. Minezawa and M. S. Gordon, J. Phys. Chem. A **115**, 7901 (2011).

[13] N. Minezawa and M. S. Gordon, J. Chem. Phys. **137**, 034116 (2012).

[14] Y. Harabuchi, S. Maeda, T. Taketsugu, N. Minezawa, and K. Morokuma, J. Chem. Theory Comput. **9**, 4116 (2013).

[15] X. Xu, S. Gozem, M. Olivucci, and D. G. Truhlar, J. Phys. Chem. Lett. **4**, 253 (2013).

[16] N. Minezawa, J. Chem. Phys. **141**, 164118 (2014).

[17] P. Zhou, J. Liu, K. Han, and G. He, J. Comput. Chem. **35**, 109 (2014).

[18] X. Zhang and J. M. Herbert, J. Phys. Chem. B **118**, 7806 (2014).

[19] M. Isegawa and K. Morokuma, J. Phys. Chem. A **119**, 4191 (2015).

[20] Y. Harabuchi, K. Keipert, F. Zahariev, T. Taketsugu, and M. S. Gordon, J. Phys. Chem. A **118**, 11987 (2014).

[21] L. Yue, Z. Lan, and Y.-J. Liu, J. Phys. Chem. Lett. **6**, 540 (2014).

[22] A. I. Krylov, Chem. Phys. Lett. **338**, 375 (2001).

[23] O. Vahtras and Z. Rinkevicius, J. Chem. Phys. **126**, 114101 (2007).

[24] Z. Li and W. Liu, J. Chem. Phys. **133**, 064106 (2010).

[25] Z. Li, W. Liu, Y. Zhang, and B. Suo, J. Chem. Phys. **134**, 134101 (2011).

[26] Z. Li and W. Liu, J. Chem. Phys. **135**, 194106 (2011).

[27] D. J. Rowe and C. Ngo-Trong, Rev. Mod. Phys. **47**, 471 (1975).

[28] J. S. Sears, C. D. Sherrill, and A. I. Krylov, J. Chem. Phys. **118**, 9084 (2003).

[29] T. Tsuchimochi and T. Van Voorhis, J. Chem. Phys. **142**, 124103 (2015).

[30] T. Tsuchimochi, J. Chem. Phys. **143**, 144114 (2015).

[31] S. Grimme, Chem. Phys. Lett. **259**, 128 (1996).

[32] S. Grimme and M. Waletzke, J. Chem. Phys. **111**, 5645 (1999).

[33] D. J. Rowe, Rev. Mod. Phys. **40**, 153 (1968).

[34] T. Helgaker, P. Jørgensen, and J. Olsen, *Molecular Electronic-Structure Theory* (Wiley, New York, 2000).

[35] Z. Szekeres, Á. Szabados, M. Kállaya, and P. R. Surján, Phys. Chem. Chem. Phys. **3**, 696 (2001).

[36] S. Hirata and M. Head-Gordon, Chem. Phys. Lett. **314**, 291 (1999).

[37] $E^{\mathrm{BH\&HLYP}}_{xc} = 0.5E^{\mathrm{B88}}_{x} + 0.5E^{\mathrm{HF}}_{x} + E^{\mathrm{LYP}}_{c}$.

[38] D. Maurice and M. Head-Gordon, Int. J. Quantum Chem. Symp. **29**, 361 (1995).

[39] Y. Shao, Z. Gan, E. Epifanovsky, A. T. B. Gilbert, M. Wormit, J. Kussmann, A. W. Lange, A. Behn, J. Deng, X. Feng, D. Ghosh, M. Goldey, P. R. Horn, L. D. Jacobson, I. Kaliman, R. Z. Khaliullin, T. Kús, A. Landau, J. Liu, E. I. Proynov, Y. M. Rhee, R. M. Richard, M. A. Rohrdanz, R. P. Steele, E. J. Sundstrom, H. L. Woodcock III, P. M. Zimmerman, D. Zuev, B. Albrecht, E. Alguire, B. Austin, G. J. O. Beran, Y. A. Bernard, E. Berquist, K. Brandhorst, K. B. Bravaya, S. T. Brown, D. Casanova, C.-M. Chang, Y. Chen, S. H. Chien, K. D. Closser, D. L. Crittenden, M. Diedenhofen, R. A. DiStasio, Jr., H. Dop, A. D. Dutoi, R. G. Edgar, S. Fatehi, L. Fusti-Molnar, A. Ghysels, A. Golubeva-Zadorozhnaya, J. Gomes, M. W. D. Hanson-Heine, P. H. P. Harbach, A. W. Hauser, E. G. Hohenstein, Z. C. Holden, T.-C. Jagau, H. Ji, B. Kaduk, K. Khistyaev, J. Kim, J. Kim, R. A. King, P. Klunzinger, D. Kosenkov, T. Kowalczyk, C. M. Krauter, K. U. Lao, A. Laurent, K. V. Lawler, S. V. Levchenko, C. Y. Lin, F. Liu, E. Livshits, R. C. Lochan, A. Luenser, P. Manohar, S. F. Manzer, S.-P. Mao, N. Mardirossian, A. V. Marenich, S. A. Maurer, N. J. Mayhall, C. M. Oana, R. Olivares-Amaya, D. P. O'Neill, J. A. Parkhill, T. M. Perrine, R. Peverati, P. A. Pieniazek, A. Prociuk, D. R. Rehn, E. Rosta, N. J. Russ, N. Sergueev, S. M. Sharada, S. Sharmaa, D. W. Small, A. Sodt, T. Stein, D. Stück, Y.-C. Su, A. J. W. Thom, T. Tsuchimochi, L. Vogt, O. Vydrov, T. Wang, M. A. Watson, J. Wenzel, A. White, C. F. Williams, V. Vanovschi, S. Yeganeh, S. R. Yost, Z.-Q. You, I. Y. Zhang, X. Zhang, Y. Zhou, B. R. Brooks, G. K. L. Chan, D. M. Chipman, C. J. Cramer, W. A. Goddard III, M. S. Gordon, W. J. Hehre, A. Klamt, H. F. Schaefer III, M. W. Schmidt, C. D. Sherrill, D. G. Truhlar, A. Warshel, X. Xua, A. Aspuru-Guzik, R. Baer, A. T. Bell, N. A. Besley, J.-D. Chai, A. Dreuw, B. D. Dunietz, T. R. Furlani, S. R. Gwaltney, C.-P. Hsu, Y. Jung, J. Kong, D. S. Lambrecht, W. Liang, C. Ochsenfeld, V. A. Rassolov, L. V. Slipchenko, J. E. Subotnik, T. Van Voorhis, J. M. Herbert, A. I. Krylov, P. M. W. Gill, and M. Head-Gordon, Mol. Phys. **113**, 184 (2015).

[40] F. Neese, WIREs Comput. Mol. Sci. **2**, 73 (2011).

[41] E. Epifanovsky, K. Kowalski, P.-D. Fang, M. Valiev, S. Matsika, and A. I. Krylov, J. Phys. Chem. A **112**, 9983 (2008).

[42] M. P. Fülscher, L. Serrano-Andrés, and B. O. Roos, J. Am. Chem. Soc. **119**, 6168 (1997).

[43] M. Schreiber, M. R. Silva-Junior, S. P. A. Sauer, and W. Thiel, J. Chem. Phys. **128**, 134110 (2008).

[44] M. Valiev and K. Kowalski, J. Chem. Phys. **125**, 211101 (2006).

[45] M. E. Foster and B. M. Wong, J. Chem. Theory Comput. **8**, 2682 (2012).

[46] J. C. Tully, J. Chem. Phys. **93**, 1061 (1990).

[47] D. Casanova and M. Head-Gordon, Phys. Chem. Chem. Phys. **11**, 9779 (2009).

[48] B. G. Levine, J. D. Coe, and T. J. Martínez, J. Phys. Chem. B **112**, 405 (2008).

[49] M. J. Bearpark, M. A. Robb, and H. B. Schlegel, Chem. Phys. Lett. **223**, 269 (1994).

[50] Ohio Supercomputer Center, http://osc.edu/ark:/19495/f5s1ph73 (accessed October 31, 2015).